Nanoparticle-assisted high photoconductive gain in composites of polymer and fullerene

HSIANG-YU CHEN[1], MICHAEL K. F. LO[2], GUANWEN YANG[1], HAROLD G. MONBOUQUETTE[2,3] AND YANG YANG[1,3]*

[1]Department of Materials Science and Engineering, University of California–Los Angeles, Los Angeles, California 90095, USA
[2]Department of Chemical and Biomolecular Engineering, University of California–Los Angeles, Los Angeles, California 90095, USA
[3]California NanoSystems Institute, University of California–Los Angeles, Los Angeles, California 90095, USA
*e-mail: yangy@ucla.edu

Published online: 27 July 2008; doi:10.1038/nnano.2008.206

Polymer–inorganic nanocrystal composites[1–10] offer an attractive means to combine the merits of organic and inorganic materials into novel electronic and photonic systems. However, many applications of these composites are limited by the solubility[11] and distribution of the nanocrystals in the polymer matrices. Here we show that blending CdTe nanoparticles into a polymer–fullerene matrix followed by solvent annealing[12] can achieve high photoconductive gain under low applied voltages. The surface capping ligand renders the nanoparticles highly soluble in the polymer blend, thereby enabling high CdTe loadings. An external quantum efficiency as high as ~8,000% at 350 nm was achieved at −4.5 V. Hole-dominant devices coupled with atomic force microscopy images show a higher concentration of nanoparticles near the cathode–polymer interface. The nanoparticles and trapped electrons assist hole injection into the polymer under reverse bias, contributing to efficiency values in excess of 100%.

Photoconductivity gain is desirable for highly sensitive photodetectors, and impact ionization[13] has been widely used in inorganic photodetectors to achieve this. However, organic materials do not normally exhibit impact ionization due to their disordered structure, which cannot form a band with extended states as in inorganic materials[14]. Carriers within organic materials are thus more localized and charge transport occurs through thermal-activated hopping. As a result, it is difficult for carriers in organic materials to accumulate sufficient kinetic energy before their next collision to enable an avalanche effect. In 1994, photoconductive gain was discovered in an organic perylene pigment film[15]. The mechanism for this has been attributed to the trapped holes near the organic film/electrode interface improving the tunnelling injection of electrons, resulting in photoconductive gain. This discovery is an important breakthrough, as it provides a route for organic materials to be used in highly sensitive photodetectors while preserving the advantages of organic materials. Recently, a high photoconductive gain has been reported for films of the small organic molecule, F_{16}CuPc (Pc: phthalocyanine), under low bias[16]. Although polymers would present advantages of easy processing, flexibility with regard to additive concentration, and controllable morphology by solvent selection, high photoconductive gain under small bias has not yet been realized for organic polymer films. Photoconductive gain has been found in both pure polymer[17,18] and polymer/nanoparticle blend systems[19], but a rather high voltage is needed to achieve high photoconductive gain, which limits the applications of these systems. In this manuscript, we show that by using the advantages of both polymers and nanoparticles (tunable optical and electrical properties), high photoconductive gain under small bias can be achieved with a simple polymer/nanoparticle blend film sandwiched between two metal electrodes.

In our system, a P3HT (poly(3-hexylthiophene)):PCBM((6,6)-phenyl-C_{61}-butyric acid methyl ester) polymer matrix film is doped with CdTe nanoparticles, which are capped with *N*-phenyl-*N*′-methyldithiocarbamate (PMDTC) (Fig. 1a). The CdTe nanoparticles with PMDTC capping ligand are highly soluble in dichlorobenzene (DCB), which is also a good solvent for polymer blends. No NP aggregates are observed, even at a concentration as high as ~30% (300 mg ml^{-1}) in DCB. Devices made from this polymer/nanoparticle blend display high photoconductive gain (EQE ≈ 8,000%) when the film is reverse-biased at less than −5 V. To our knowledge, this is the highest photoconductive gain obtained so far in a polymer-based system under such low applied voltages.

All devices reported in this manuscript are of the structure shown in Fig. 1a, with the active layer composed of P3HT:PCBM with (devices B, B2 and B3) or without (device A) CdTe nanoparticles. The solutions and devices that were investigated are listed in Table 1, 2 (see Methods for processing details). The current density/voltage (J–V) characteristics of devices A and B are shown in Fig. 1b. Device A shows typical polymer solar cell characteristics[12], but the dark current of device B in the forward bias region is significantly suppressed, although a clear diode characteristic is still observed (Fig. 1c). The photovoltaic property almost disappears, but with a higher applied voltage in reverse bias, the photocurrent of device B changes sharply to a much higher value than device A. A reverse-bias photocurrent density as high as 952 mA cm^{-2} is observed at −5 V.

The absorption spectra of the polymer films in devices A, B and C are shown in Fig. 1d, with the absorption of CdTe nanoparticles and PMDTC in DCB shown in the inset. For direct comparison, the films used for absorption measurements were controlled to be of about the same thickness. No obvious absorption change was observed when PMDTC was blended with P3HT:PCBM (devices A and C), but increased absorption for wavelengths longer than

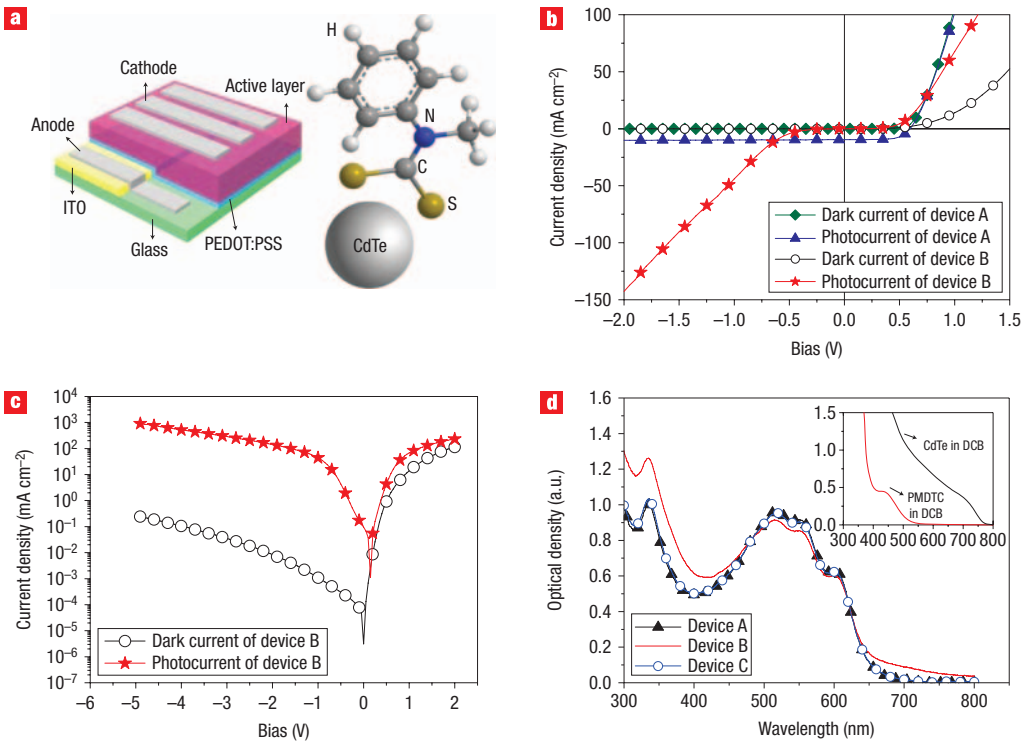

Figure 1 Device structure, current density/voltage (*J–V*) characteristics and absorption spectrum. a, Device structure and chemical structure of the PMDTC ligand (not to scale). **b**, The *J–V* curve of devices A (without CdTe NPs) and B (with CdTe NPs). Significant photocurrent increase is observed under reverse bias when CdTe nanoparticles are blended into the P3HT:PCBM matrix. **c**, The *J–V* curve of device B in logarithmic scale. A clear diode characteristic is shown by the dark current density curve. **d**, Absorption spectrum of films in devices A, B and C. PMDTC blended with P3HT:PCBM shows no obvious change in absorption. Inset: absorption spectrum of CdTe nanoparticles (with PMDTC capping ligands) and free PMDTC in DCB.

Table 1 List of solutions.

Solutions	Contents	Solvent
Solution A	2% (20 mg ml^{-1}) P3HT:PCBM (1:1 wt ratio)	DCB
Solution B	2% (20 mg ml^{-1}) P3HT:PCBM (1:1 wt ratio) with 3.1% (31 mg ml^{-1}) CdTe nanoparticles	DCB
Solution C	2% (20 mg ml^{-1}) P3HT:PCBM (1:1 wt ratio) with 2.2% (22 mg ml^{-1}) PMDTC	DCB

Table 2 List of devices with details of the conditions used.

Devices	Solution used	Solvent annealed*	Cathode
Device A	Solution A	Yes	Ca/Al
Device B	Solution B	Yes	Ca/Al
Device C	Solution C	Yes	Ca/Al
Device B2	Solution B	No†	Ca/Al
Device B3	Solution B	Yes	MoO_3(5 nm)/Al(70 nm)

*Solvent annealing was carried out by spin-coating the polymer solutions at 800 r.p.m. for 45 s and allowing the film to dry slowly in a covered petri dish until the colour of the polymer films changed from orange to deep purple.
†Solutions were spin-coated at 800 r.p.m. for 95 s.

650 nm and shorter than 450 nm were observed in device B. Other measurements of device C were carried out to exclude the possible contribution of PMDTC to the photoconductive gain (see Supplementary Information).

Three vibronic shoulders (at ~515, 550 and 610 nm), representing strong interchain–interlayer interactions of P3HT[12,20], are preserved in the absorption spectra after blending in CdTe nanoparticles. This implies that the high concentration CdTe nanoparticles does not hinder the stacking of P3HT under solvent annealing, which is important for achieving high carrier mobility[21]. Transmission electron microscopy (TEM) images of the film (Fig. 2a) represent highly condensed aggregates of CdTe nanoparticles. It is worth mentioning that these aggregates have thread-like features (inset of Fig. 2a), which have not been observed in previously reported TEM images of nanoparticles with other capping ligands in polymer films[3,10,22].

The EQE of device B at different wavelengths is shown in Fig. 2b. EQE values higher than 100% are observed at an applied voltage of only −1 V. With increasing negative bias, EQEs as high as ~8,000% at 350 nm and ~600% at 700 nm are reached at voltages of −4.5 V. An EQE higher than 100% implies that extra charges are generated in the devices. In this system, these extra charges are likely to be injected from the external circuit. The possibility of multiple exciton[23] generation by one photon is rather low because the photonic energy is not high enough for this process[7]. The EQE of device A measured under the same conditions is shown in Fig. 2c for comparison.

The relative energy levels of P3HT, PCBM and PMDTC were determined by cyclic voltammetry and are shown in the inset of Fig. 3a. For the CdTe core, we used the values calculated by Dayal and colleagues[24] for CdTe nanoparticles of about the same size (~8 nm diameter). Note that the electron affinity of CdTe nanoparticles likely differs based on the different preparation

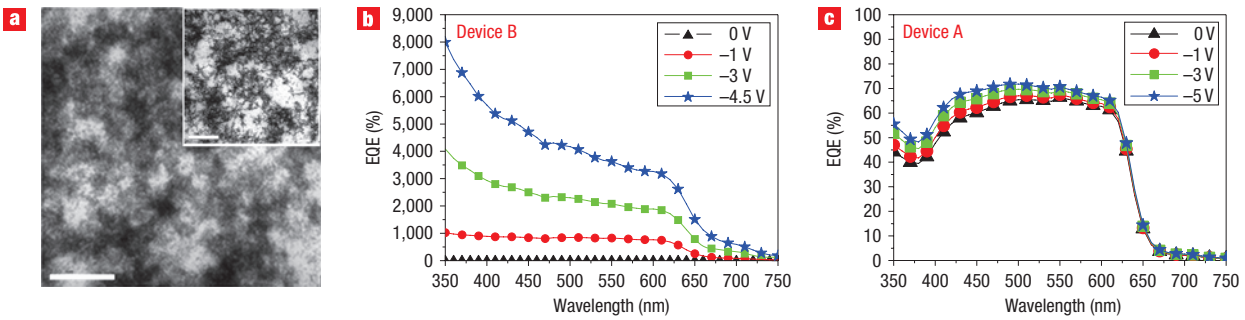

Figure 2 TEM images and external quantum efficiency. a, TEM images of P3HT:PCBM/CdTe nanoparticles (concentration of CdTe nanoparticles, ~3.1% (31 mg ml^{-1})) film. The scale bars in the main image and the inset are 200 nm and 1 μm, respectively. The solution was drop cast onto a TEM grid for sample preparation. Highly condensed aggregates of CdTe nanoparticles are observed and thread-like features are clearly visible in the inset. **b**, EQE values of device B under zero and reverse bias. A value of more than 100% is obtained under reverse bias, even at the absorption edge of CdTe nanoparticles (~700 nm). **c**, EQE values of device A measured under the same conditions.

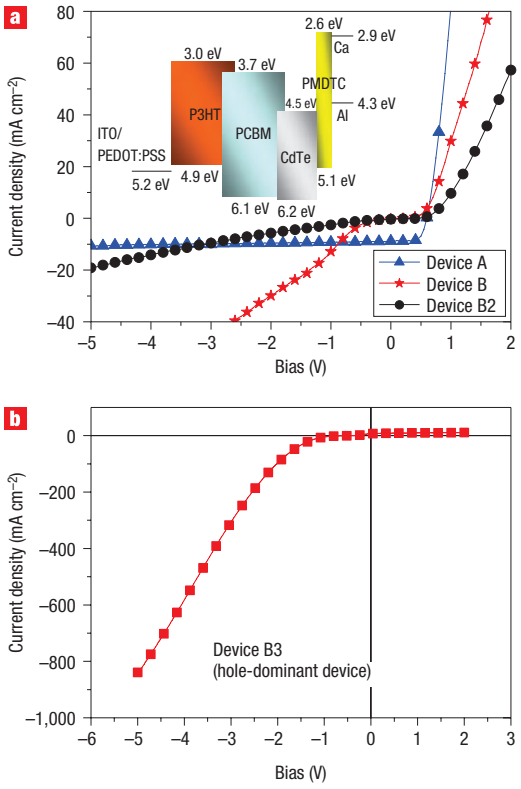

Figure 3 Photocurrent density/voltage characteristic of different devices. a, *J*–*V* curve of devices A, B and B2 (without solvent annealing). A much higher photocurrent density in reverse bias is observed for device B, whereas the increase of photocurrent density is much slower in device B2. Inset: relative energy diagram of all the materials used in this manuscript. **b**, *J*–*V* curve of device B3 (after solvent annealing, hole-dominant device, with a MoO_3(5 nm)/Al(70 nm) electrode) under light exposure. A much higher photocurrent density is observed under reverse bias (while the MoO_3/Al electrode is positively biased).

methods. Recently, it has been found that the measured energy level of nanocrystals varies significantly with different surface capping group[25]. To remove the surface ligand effect, here we instead use a calculated value[24] for the CdTe core. According to this energy diagram, CdTe nanoparticles act as deep electron traps in this system. Under exposure to light, excitons are generated in CdTe nanoparticles when the wavelength is shorter than its absorption edge, ~750 nm. From the relative energy level, the exciton generated at the core of the nanoparticles may lose its hole to the PMDTC ligand. This scenario agrees with the observed absence of CdTe nanoparticle photoluminescence (PL) in DCB when the capping ligand is changed from oleic acid to PMDTC.

We thus speculate that the ability of CdTe nanoparticles to trap electrons under illumination leads to photo-induced carrier injection from the cathode, which results in a measured EQE much greater than 100%. To clarify the role of CdTe nanoparticles, we made another device, device B2 (the same as device B, but without solvent annealing; see Table 2). The *J*–*V* curve of device B2 is compared with devices A and B in Fig. 3a. The photocurrent of device B2 under reverse bias is much lower than that of device B. These data suggest that the morphology of the polymer/nanoparticle system is also significant for this high photoconductive gain, and is not simply due to the addition of CdTe nanoparticles. Note that from the *J*–*V* curve of device B2, a photoconductive gain is expected only when higher bias is applied. A similar phenomenon has been recently observed by others[19]. In that work, PbSe quantum dots and PCBM were each blended with polymer, and a conductive gain was obtained for both systems under higher reverse bias. The photoconductive gain was attributed to the photogenerated electrons being trapped by either PbSe quantum dots or PCBM in the 'bulk', which caused the injection of hole carriers from the external circuit.

To better understand the function of solvent annealing in our system, a hole-dominant device (device B3; see Table 2) was studied. In our devices, forward bias is defined as indium tin oxide (ITO) positively biased. Under reverse bias, holes were injected from the MoO_3/Al electrode of device B3. A photocurrent density of 838 mA cm^{-2} was observed at −5 V, which is much higher than that under forward bias (Fig. 3b). The much higher hole injection from MoO_3/Al to the polymer blend implies that the injection barrier between the MoO_3/Al electrode and the polymer blend is much lower than that of the ITO(PEDOT)/polymer contact. Devices without CdTe nanoparticles are made simultaneously under the same conditions, but no similar phenomenon was observed.

The much higher photocurrent of device B3 in reverse bias than in forward bias also implies that the distribution of CdTe

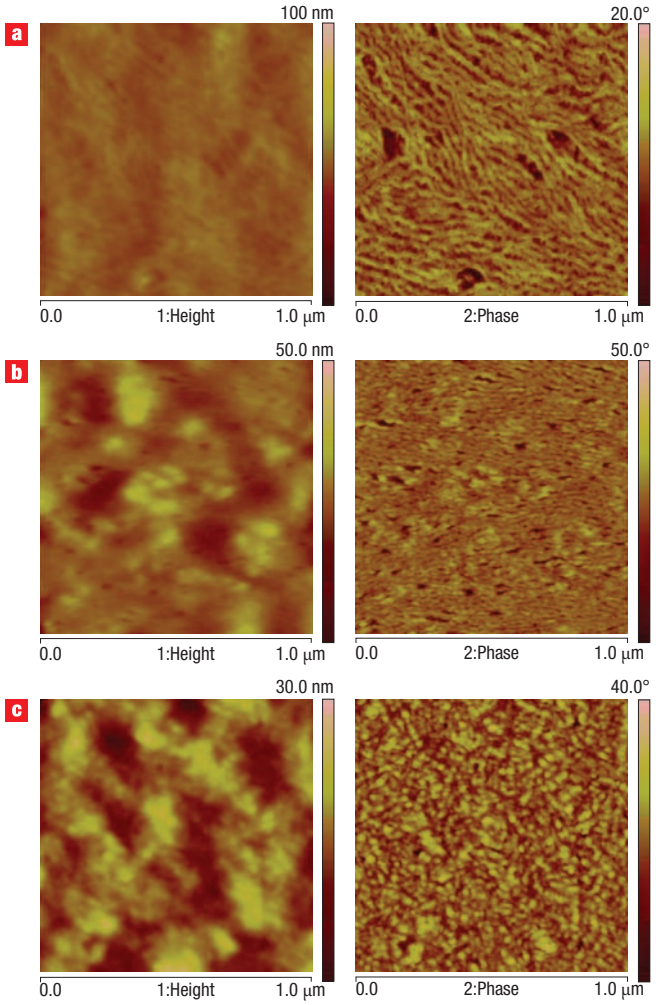

Figure 4 Tapping-mode AFM images of the polymer films. Topography (left) and phase images (right) of device A (**a**), B2 (**b**) and B (**c**) in 1 μm × 1 μm. The phase images of devices A and B2 show a fibrillar structure, whereas device B presents an island-like surface morphology. The absence of fibrillar structure in the surface morphology of device B is a result of adding nanoparticles coupled with the solvent annealing process.

nanoparticles along the direction normal to the film may not be uniform; that is, the concentration may be higher near the polymer blend/MoO_3 interface, which lowers the injection barrier for holes injected from the MoO_3 into the polymer blend layer. A similar aggregation of NPs on the top of polymer films has also been observed in polymer light-emitting diodes[26]. For comparison, a hole-dominant device made without solvent annealing does not show a similar effect and the J–V curve looks symmetric. According to these observations, it is very likely that the concentration of CdTe nanoparticles is higher near the polymer blend/MoO_3 interface as a result of solvent annealing.

Tapping-mode atomic force microscopy was used to further study the surface topography and phase images of the films of devices A, B and B2 (Fig. 4a–c), which are normally in direct contact with the cathodes (Ca/Al or MoO_3/Al) in the devices. Long fibrillar structures are clearly observed in the phase image of the polymer film in device A (Fig. 4a, right), whereas the film in device B2 (Fig. 4b, right) represents a similar structure but with shorter and less ordered fibrillar segments. This fibrillar structure represents the crystalline domains of P3HT (ref. 12). However, the film in device B provides a very different phase image (Fig. 4c, right), in that island-like structures appear instead of fibrillar features. These images show that the surface morphology change is a result of adding nanoparticles coupled with the solvent annealing process. The concentration of CdTe nanoparticles near the 'top' of the polymer blend film is likely to be higher, yielding a totally different morphology.

To conclude, a solvent annealing step after film spin-coating is likely to give rise to a higher concentration of CdTe nanoparticles on the top of the annealed film. Under light exposure, CdTe nanoparticles with photo-induced trapped electrons thus lower the hole injection barrier from the top electrode to the P3HT film. Therefore, CdTe nanoparticles behave as a valve that controls hole injection under reverse bias. The contribution to the photoconductive gain can be from both the nanoparticles near the top surface of the polymer film and in the bulk[19]. Judging from our data, nanoparticles near the top surface might play a dominant role. An EQE value higher than 100% at the absorption edge of the CdTe nanoparticles (~700 nm) suggests that significant charge injection already occurs. At the onset of P3HT absorption (~650 nm), more excited electrons are generated in the P3HT, resulting in more electrons being trapped in the nanoparticles and thus an even higher charge injection rate. With this polymer/nanoparticle blend system, a high photoconductive gain can be obtained over the absorption range of the polymer and nanoparticles.

METHODS

SOLUTION PREPARATION

Solution A consists of 2% (20 mg ml^{-1}) P3HT:PCBM (1:1 weight ratio) in DCB solvent. Solution B was made by mixing P3HT:PCBM solution with CdTe nanoparticles and the concentration of CdTe nanoparticles after mixing was ~3.1% (31 mg ml^{-1}). Solution C was made by mixing P3HT:PCBM solution and PMDTC and the concentration of PMDTC after mixing was ~2.2% (22 mg ml^{-1}). The concentrations of P3HT and PCBM were kept as 2% in solution B and C after mixing.

DEVICE FABRICATION

Devices A, B and C were made from solutions A, B and C, respectively. All the devices had the structure ITO/PEDOT:PSS/polymer blend/calcium (Ca)/aluminum (Al) except device B3. (PEDOT:PSS is poly(ethylenedioxythiophene):polystyrene sulphonate.) A PEDOT:PSS layer was pre-coated onto the ITO substrate before spin-casting the solutions. All solutions were spin-coated at 800 r.p.m. for 45 s. The thicknesses of the polymer films, measured with a Dektak 3030 profilometer, for devices A, B and C were ~215 nm, 255 nm and 225 nm, respectively. After spin-coating, the wet polymer films were left to dry slowly in petri dishes until the colour of the polymer films changed from orange to purple. This slow growth (or solvent annealing) process was previously demonstrated[12] to achieve an optimized morphology for solar cell devices. Thermal annealing at 110 °C for 10 min was then carried out on device A before deposition of the electrodes from evaporated metal. A bilayer cathode consisting of a calcium layer (20 nm) and subsequently an aluminium layer (100 nm) was deposited by thermal evaporation under vacuum (1×10^{-6} torr). The active area for all the devices discussed here was ~12 mm^2. Device B2 was made by spin-coating solution B at 800 r.p.m. for 95 s to ensure the film was dry (the colour of the polymer film does not change with time after spin-coating).

EXPERIMENTAL CONDITIONS

The current density/voltage (J–V) characteristics were measured using a Keithley 2400 source-measuring unit. A calibrated solar simulator (Oriel) with 100 mW cm^{-2} power density was used as the light source. In addition, the EQE was used to determine the device photo response as a function of wavelength, where EQE is defined as the number of charge carriers collected per incident photon at a specific wavelength. In the EQE measurement, a xenon lamp (Oriel, model 66150, 75 W) was used as the light source, and a chopper and

lock-in amplifier were used for phase-sensitive detection. The wavelength was controlled by a monochrometer. To ensure accurate counting of the incident photons, a calibrated silicon photodiode was used as a reference device.

Received 27 April 2008; accepted 19 June 2008; published 27 July 2008.

References

1. Huynh, W. U., Dittmer, J. J. & Alivisatos, A. P. Hybrid nanorod–polymer solar cells. *Science* **295,** 2425–2427 (2002).
2. Sun, B. & Greenham, N. C. Improved efficiency of photovoltaics based on CdSe nanorods and poly(3-hexylthiophene) nanofibers. *Phys. Chem. Chem. Phys.* **8,** 3557–3560 (2006).
3. Han, L. *et al.* Synthesis of high quality zinc-blende CdSe nanocrystals and their application in hybrid solar cells. *Nanotechnology* **17,** 4736–4742 (2006).
4. Zhou, Y. *et al.* Hybrid nanocrystal/polymer solar cells based on tetrapod-shaped $CdSe_xTe_{1-x}$ nanocrystals. *Nanotechnology* **17,** 4041–4047 (2006).
5. Beek, W. J. E., Wienk, M. M. & Janssen, R. A. J. Efficient hybrid solar cells from zinc oxide nanoparticles and a conjugated polymer. *Adv. Mater.* **16,** 1009–1013 (2004).
6. Mcdonald, S. A. *et al.* Solution-processed PbS quantum dot infrared photodetectors and photovoltaics. *Nature Mater.* **4,** 138–142 (2005).
7. Qi, D., Fischbein, M., Drndic, M. & Selmic, S. Efficient polymer–nanocrystal quantum-dot photodetectors. *Appl. Phys. Lett.* **86,** 093103-1–3 (2005).
8. Cui, D., Xu, J., Zhu, T., Paradee, G. & Ashok, S. Harvest of near infrared light in PbSe nanocrystal–polymer hybrid photovoltaic cells. *Appl. Phys. Lett.* **88,** 183111-1–3 (2006).
9. Choudhury, K. R., Sahoo, Y., Ohulchanskyy, T. Y. & Prasad, P. N. Efficient photoconductive devices at infrared wavelengths using quantum dot–polymer nanocomposites. *Appl. Phys. Lett.* **87,** 073110-1–3 (2005).
10. Greenham, N. C., Peng, X. & Alivisatos, A. P. Charge separation and transport in conjugated-polymer semiconductor–nanocrystal composites studied by photoluminescence quenching and photoconductivity. *Phys. Rev. B* **54,** 17628–17637 (1996).
11. Huynh, W. U., Dittmer, J. J., Libby, W. C., Whiting, G. L. & Alivisatos, A. P. Controlling the morphology of nanocrystal–polymer composites for solar cells. *Adv. Funct. Mater.* **13,** 73–79 (2003).
12. Li, G. *et al.* 'Solvent annealing' effect in polymer solar cells based on poly(3-hexylthiophene) and methanofullerenes. *Adv. Funct. Mater.* **17,** 1636–1644 (2007).
13. Sze, S. M. *Physics of Semiconductor Devices* (Wiley, New York, 1981).
14. Caserta, G., Rispoli, B. & Serra, A. Space-charge-limited current and band structure in amorphous organic films. *Phys. Stat. Sol.* **35,** 237–248 (1969).
15. Hiramoto, M., Imahigashi, T. & Yokoyama, M. Photocurrent multiplication in organic pigment films. *Appl. Phys. Lett.* **64,** 187–189 (1994).
16. Reynaert, J., Arkhipov, V. I., Heremans, P. & Poortmans, J. Photomultiplication in disordered unipolar organic materials. *Adv. Funct. Mater.* **16,** 784–790 (2006).
17. Marks, R. N., Halls, J. J. M., Bradley, D. D. C., Friend, R. H. & Holmes, A. B. The photovoltaic response in poly(p-phenylene vinylene) thin film devices. *J. Phys. Condens. Matter.* **6,** 1379–1394 (1994).
18. Daubler, T. K. & Neher, D. Efficient bulk photogeneration of charge carriers and photoconductivity gain in arylamino–PPV polymer sandwich cells. *Phys. Rev. B* **59,** 1964–1972 (1999).
19. Campbell, I. H. & Crone, B. K. Bulk photoconductive gain in poly(phenylene vinylene) based diodes. *J. Appl. Phys.* **101,** 024502-1–5 (2007).
20. Sirringhaus, H. *et al.* Two-dimensional charge transport in self-organized, high-mobility conjugated polymers. *Nature* **401,** 685–688 (1999).
21. Li, G. *et al.* High-efficiency solution processable polymer photovoltaic cells by self-organization of polymer blends. *Nature Mater.* **4,** 864–868 (2005).
22. Choi, S. H. *et al.* Synthesis of size-controlled CdSe quantum dots and characterization of CdSe-conjugated polymer blends for hybrid solar cells. *J. Photochem. Photobiol. A: Chem.* **179,** 135–141 (2006).
23. Schaller, R. D., Agranovich, V. M. & Klimov, V. I. High-efficiency carrier multiplication through direct photogeneration of multi-excitons via virtual single-exciton states. *Nature Phys.* **1,** 189–194 (2005).
24. Dayal, P. B., Mehta, B. R. & Paulson, P. D. Spin–orbit splitting and critical point energy at Γ and L points of cubic CdTe nanoparticles: effect of size and nonspherical shape. *Phys. Rev. B* **72,** 115413-1–6 (2005).
25. Soreni-Harari, M. *et al.* Tuning energetic levels in nanocrystal quantum dots through surface manipulations. *Nano Lett.* **8,** 678–684 (2008).
26. Coe, S., Woo, W., Bawendi, M. & Bulovic, V. Electroluminescence from single monolayers of nanocrystals in molecular organic devices. *Nature* **420,** 800–803 (2002).

Supplementary Information accompanies this paper at www.nature.com/naturenanotechnology.

Acknowledgements

H.-Y.C. and Y.Y. acknowledge financial support from Solarmer Energy (grant no. 20061880) and the Air Force Office of Scientific Research (FA9550-07-1-0264). Help from Hyun Cheol Lee for the TEM images and valuable discussions with Gang Li from Solarmer Energy are also highly appreciated. H.-Y.C. is grateful to Wei Lek Kwan and Bao Lei for helping with the transient measurements.

Author contributions

H.-Y.C. conceived and performed the experiments and measurements. M.K.F.L. performed synthesis of CdTe nanoparticles and the capping ligands. G.Y. performed the AFM imaging. H.G.M. and Y.Y. conceptualized and directed the research project. All authors discussed the results and commented on the manuscript.

Author information

Reprints and permission information is available online at http://npg.nature.com/reprintsandpermissions/. Correspondence and requests for materials should be addressed to Y.Y.